Journal of Experimental Botany, Vol. 00, No. 0 pp. 1–12, 2026
https://doi.org/10.1093/jxb/eraf512 Advance Access Publication 26 November 2025

RESEARCH PAPER

Helical growth of twining common bean is associated with longitudinal, not skewed, microtubule patterning

Angelique A. Acevedo[1], Mariane S. Sousa-Baena[2], and Joyce G. Onyenedum[1,*]

[1] Department of Environmental Studies, New York University, New York, NY 10003, USA
[2] Botany Department, Federal University of Rio Grande do Sul, Porto Alegre, RS 91501-970, Brazil

* Correspondence: jgo5750@nyu.edu

Received 30 May 2025; Accepted 14 November 2025

Editor: James Murray, Cardiff University, UK

Abstract

Organ chirality in plants has been linked to cytoskeletal organization, as demonstrated in Arabidopsis twisted mutants, where left-skewed cortical microtubules are associated with right-handed twisting, and vice versa. While this phenotype seemingly mirrors vining habits, the hypothesis remains understudied within naturally twining plants. Qualitative observations have identified skewed microtubules in the twining stem of *Ipomoea nil* (L.) Roth vine, suggesting parallels with Arabidopsis studies. To further investigate organ chirality in twining plants, we used common bean vine (*Phaseolus vulgaris* L.) to examine the relationship between microtubule orientation, cell morphogenesis, and the right-handed twining phenotype via immunolabeling techniques. Here, we report a transition from mixed microtubule orientations in emergent and elongating internodes to a predominance of longitudinal microtubules in straight and twined stem segments post-elongation. Additionally, we report a distinction in epidermal cell shapes, where straight portions of the stem consist of lobes with rectangular cells and furrows with round cells, while twined portions comprise cells that are relatively more rectangular and stretched. We propose that these orientations reflect dynamic microtubule responses to external stimuli and growth cues, such as tensile stresses from climbing or tissue expansion. Taken together, these findings highlight dissimilarities between twisting Arabidopsis mutants and naturally twining plants.

Keywords: cell morphogenesis, climbing plants, common bean, microtubules, *Phaseolus vulgaris*, tensile stress, twining, twisting.

Introduction

Twining vines provide an opportunity to understand the developmental mechanisms underlying rapid directional growth in plants, given the uniquely dynamic movements characterizing their growth form (Sousa-Baena *et al.*, 2021). While it is known that most twining vines coil in a right-handed fashion (Edwards *et al.*, 2007; Zhou *et al.*, 2019), the cellular underpinnings that constitute handedness in naturally twining species remain understudied. At present, insights into organ handedness have primarily come from microtubule mutants in the model species Arabidopsis. These studies converge on a growing consensus that twisted organ growth (twisting roots, hypocotyl, leaf petioles, and petals) is correlated with skewed microtubules in the following way: left-handed microtubules serve as the track for left-handed cellulose microfibrils, which permits cells to grow in a right-handed direction, and vice versa. This pattern has been found in several mutants, including

spiral1 (*spr1*), *tortifolia1/spiral2* (*tor1/spr2*), *tortifolia2* (*tor2*), and *lefty* mutants (Furutani *et al.*, 2000; Thitamadee *et al.*, 2002; Buschmann *et al.*, 2004, 2009; Nakajima *et al.*, 2004; Shoji *et al.*, 2004). However, exceptions to this pattern exist, such as the *spr1-6* mutant, where right-handed twisting organs exhibited transverse and right-handed microtubules (Sedbrook *et al.*, 2004). More generally, skewed microtubules have also been observed in the straight elongation zone of roots (Liang *et al.*, 1996). These exceptions emphasize the complex relationship between microtubules and organ-level twisting as a result of typical microtubule variability and dynamics.

While other components of the cell wall, like rhamnogalacturonan (RG-I) pectins, have been shown to affect plant cell patterning, as shown in the *RHM1* (*rmh1-1*) Arabidopsis mutant (Saffer *et al.*, 2017), most research has focused on the link between cellulose microfibrils and cell expansion. Cellulose is the primary load-bearing element of the cell wall, constraining maximal cell expansion perpendicular to the net cell orientation (Baskin, 2005; Anderson *et al.*, 2010; Buschmann and Borchers, 2020). However, this net constraint is often transformed by the dynamic behavior of cortical microtubules, which self-organize beneath the plasma membrane to guide cellulose synthase complexes and orient the deposition of cellulose layers in the plant cell wall (Heath, 1974; Paredez *et al.*, 2006; Duncombe *et al.*, 2022). When microtubule orientation—and consequently cellulose arrangement—is random across the cell axis, cell expansion is termed isotropic (uniform), whereas unidirectional microtubule orientation is termed anisotropic (directional) due to unequal yielding of the cell wall (Green, 1962). Generally, plant cells can undergo both isotropic and anisotropic growth. Prolonged isotropic expansion typically produces rounded cells, while prolonged anisotropic expansion produces elongated cell morphologies, and yet it is the combination and assortment of these uniquely shaped cells forming plant organs that makes them an area of interest for investigating twisted organs.

Despite the well-documented role of microtubule orientation in modulating cell anisotropy and organ-twisting of Arabidopsis mutants, its role in naturally twining species remains understudied. Sousa-Baena *et al.* (2021) provided an initial qualitative analysis performed on a twining vine, *Ipomoea nil* (L.) Roth, which revealed skewed microtubule orientation in fully twined internodes, drawing parallels to the work in Arabidopsis. In this study, we aim to clarify and deepen our understanding of the relationship between cortical microtubules and right-handed twining by using common bean vine, *Phaseolus vulgaris* L. (Fabaceae). We report the counterintuitive finding that a longitudinal—rather than a left- or right-skewed—microtubule orientation dominates in twined internodes. Furthermore, we identified a link between stem segment morphology and cell shape, whereby straight stem segments display alternating lobes with elongated rectangular cells and furrows with rounded cells, and twined internodes consisted of cells possessing a stretched quality. Our results highlight an important distinction between the development of twining in vines, which requires internodes to elongate and grow in contact with a support, versus twisted Arabidopsis mutants, where twisting occurs at the level of the cell.

Materials and methods

Plant materials and growing conditions

In this study, we selected *Phaseolus vulgaris* L. RIL L88-57 as a model system to investigate the cellular mechanisms underlying twining. To improve the success and uniformity of seed germination, all seeds were imbibed for 24 h in 20% (w/v) polyethylene glycol (PEG) 4000 in the dark and thoroughly rinsed with deionized water. After rinsing, seeds were transferred to Petri dishes containing dampened 90 mm-diameter Whatman filter paper (GE Healthcare Life Sciences, cat. no. 1001-090) for 2–4 d at room temperature in indirect bright light until the radicle emerged.

Germinated seeds were then transferred to 475 ml (10 cm) pots containing Lambert LM-111 All Purpose soil mix (cat. no. 664980 2510). L88-57 plants were grown under 12 h light conditions at ~130 μmol m^{-2} s^{-1} PAR, followed by a 30 min ramp-down period to a 12 h dark cycle and repeating with a 30 min ramp-up back to the light cycle. Pots were positioned ~76 cm below LED light panels in Environmental Growth Chambers (EGC models GR48 and SLR-90) with conditions set to 50% relative humidity and a temperature of 24 °C. Plants were also supplemented with 75 ppm of Jack's Professional 20-20-20 General Purpose fertilizer containing micronutrients.

Selection of morphological stages

To understand the relationship between microtubule angles, cell morphogenesis, and plant morphology, we sampled plants at key biomechanical stages (*sensu* Onyenedum *et al.*, 2025): stage 1 plants are erect seedlings with embryonic leaves; stage 2 plants have a slight bend of the epicotyl with internode development; stage 3 is characterized by the small revolutions of the shoot apex, known as 'regular circumnutation'; stage 4 marks a period of internode elongation and 'exaggerated circumnutation'; and stage 5 is defined by a plant's twined position. We focused on stages 2, 3, and 5 for their distinct biomechanical features and habits, representing critical developmental periods necessary for twining.

At these stages, we selected three internodes to investigate, in addition to the hypocotyl, which served as a comparable reference to previous microtubule studies conducted on Arabidopsis hypocotyls. Selected internodes provided unique insights into the basal, central, and twined regions of a developing plant. Internode 1 remained stationary and relatively short throughout stages 2, 3, and 5. Internode 3 acted as a transition zone, facilitating circumnutational movements observed in stage 3 before becoming straight and stationary at stage 5. Similarly, internode 6 participated in circumnutation at stage 3, but settled into a twined stationary position at stage 5.

Microtubule immunolabeling

To characterize microtubule patterning across key biomechanical stages of twining, we labeled epidermal peels with an anti-tubulin antibody and tracked microtubule arrangement via confocal microscopy. Epidermal peels were prepared by nicking the surface of a fresh internode with an Astra Double Edge razor, then gently grasping the epidermal flap with blunt-ended tweezers and pulling straight downwards as described in Medina *et al.* (2022). A minimum number of three individuals were sampled, focusing on their hypocotyl and internodes 1, 3, and 6 at the three key developmental stages, stage 2, stage 3, and stage 5.

Microtubules were labeled using protocols adapted from Wasteneys *et al.* (1997) and Celler *et al.* (2016) with modifications for *Phaseolus vulgaris* tissue. Thin epidermal peels from selected internodes were fixed for

40 min in a 0.5% glutaraldehyde and 1.5% formaldehyde solution before being washed three times for 10 min in PMET buffer (50 mM PIPES, 5 mM EGTA, 1 mM magnesium sulfate, and.05% Triton X-100, pH 7.2). The samples were then placed between two plain non-frosted microscope slides (VWR, cat. no. 48300-026), secured by two heavy-duty spring clamps, and flash-frozen by being dipped in a bath of liquid nitrogen with tongs. Once frozen, the slides were directly transferred to a −80 °C aluminum block and crushed with enough force to generate noticeable cracks along the peel. The slides were immediately pulled apart and placed onto a room-temperature aluminum block to thaw. This freeze–thaw cycle was repeated by dipping the slides into liquid nitrogen a second time. Samples were then incubated in a cell wall digestion enzyme solution for 30 min [0.05% pectolyase from *Aspergillus japonicus*, 0.4 M D-mannitol, 1% BSA in 1X phosphate-buffered saline (PBS)]. Following the digestion solution, samples were washed three times for 10 min in PMET buffer and left to incubate for 3 h at room temperature in permeabilization buffer (1% Triton X-100 in 1X PBS, pH 7.5) on a variable-speed rocker.

Further, samples were washed three times for 10 min in 1X PBS solution and transferred to a sodium borohydride solution for 20 min (1 mg ml^{-1} sodium borohydride in 1X PBS). The sodium borohydride solution was discarded and replaced with a blocking buffer for 30 min (1% BSA, 50 mM glycine in 1X PBS). A primary antibody solution of mouse anti-α-tubulin B 512 (Krackeler Scientific Inc., Albany, NY, USA, cat. no. 45-T6074-200UL-EA) in blocking buffer was used at a 1:1000 dilution to incubate peels for ∼14–16 h in 1.5 ml microfuge tubes at 4 °C. Subsequently, samples were rinsed five times for 10 min each with an incubation buffer in Petri dishes on a variable-speed rocker (50 mM glycine in 1X PBS). They were then placed into a blocking buffer for 30 min. Next, a secondary antibody solution, using Alexa 488-conjugated goat anti-mouse IgG (Thermo Fisher Scientific, cat. no. A28175), was prepared at a 1:100 dilution in blocking buffer and used to incubate the samples at room temperature for 3 h in the dark. Samples were then removed from the secondary antibody solution and washed three times for 10 min in 1X PBS on the rocker. Finally, peels were mounted in Citifluor™ AFI Antifading Mountant Solution with a coverslip and sealed the edges with fast-drying Sally Hansen top-coat nail polish.

Microtubule images were acquired using a Leica Stellaris 5/DMi8 confocal model with an inverted microscope at ×20 and ×63/1.4 NA oil immersion objectives with a ×2 zoom factor (excitation 488 nm, emission 510–530 nm range). Z-stacks were created to view cells from cortical to epidermal layers with a median noise reduction filter and later used to generate projections of the outermost periclinal side of the cell's surface. These projections were imported into Adobe Photoshop and rotated to align the cells vertically, providing an upright longitudinal view. Next, the projections were processed with ImageJ using the FibrilTool plugin following the installation and fibril quantification process of Boudaoud *et al.* (2014). For each internode and individual ($n \geq 3$ biological replicates) across developmental stages, 30 epidermal cells were measured per biological replicate. Microtubules angled between 0–22.5° and 157.5–180° were labeled transverse, while angles at 90° within a ±22.5° range were labeled longitudinal. Microtubules angled between 22.5° and 67.5° were categorized as right-skewed, and those between 112.5° and 157.5° were categorized as left-skewed. Grouping of microtubule angle bins was based on previous CMT classification studies (Renou *et al.*, 2024).

Barplot visualization of these data was completed using ggplot2 (v3.5.1; Wickham, 2016), ggpubr (v0.6.0; FC *et al.*, 2022), and ggpatterns (v1.1.4; Kassambara, 2023) packages.

Stem morphology and classifying cell morphologies

To describe bean stem morphology in Figure 4, we stained stem cross sections of the hypocotyl, internode 1, internode 3, and internode 6 with Pontamine fast scarlet 4B (S4B; Anderson et al. 2010), also known as Direct Red 23. A 0.01% (w/v) solution of S4B, was prepared in 1X PBS and used to incubate epidermal peels for 40 minutes in a 1.5 mL tube. During this period, peels were stored away in dark area. Peels were then washed three times in 1X PBS for 5 minutes each and vigorously shaken using a Vortex-Genie 2. Finally, the samples were mounted in 1X PBS, sealed with a coverslip and a fast-drying Sally Hansen top-coat nail polish. Panoramic confocal images were taken using the Leica Stellaris 5/DMi8 confocal model with an inverted microscope and with a 20X dry objective at a 2X zoom factor. S4B was detected at an excitation of 532 nm and captured in the 590–620 nm emissions range." To characterize cell morphogenesis through key biomechanical stages, we used propidium iodide (PI) to stain epidermal cells and morphologically segment their cell walls via the MorpholibJ plugin of ImageJ. PI was prepared as a stock solution of 1 mg ml^{-1} in deionized water (stored at 4 °C) before being further diluted into a 10 µg ml^{-1} working solution. Epidermal peels were made from fresh tissue and incubated in a 1.5 ml tube containing PI working solution for 30 min in the dark and on ice before being thoroughly washed three times for 2 min each. The tube was inverted 2–3 times and shaken using a Vortex-Genie 2.

Panoramic confocal images were generated by Leica software using the Leica Stellaris 5/DMi8 confocal microscope with a ×20 dry objective at a ×2 zoom factor. PI was detected at an excitation of 532 nm and captured in the 590–630 nm emissions range. The resulting images were imported and processed via ImageJ and the MorpholibJ plugin (Legland *et al.*, 2016). This plugin was used to morphologically segment cells (with user adjustments using the 'merge' function) and label various regions of interest with corresponding cell measurements: cell circularity, geodesic diameter, and cell area. Stomatal and trichome precursor cells were removed from the analysis. Once measurements were assigned to their corresponding region of interest labels, the label edition feature was used to generate a spectral color map. Color maps reflected cell measurements like cell 'area' and were used to create a heat map with the look-up table 'Fire' gradient.

Measurements were retrieved from ImageJ, filtered outliers removed, and converted into bar plots and boxplots using RStudio packages ggplot2 (v3.5.1; Wickham, 2016) and RColorBrewer (v1.1-3; Neuwirth, 2022) to compare the distribution of cells in furrowed and lobed portions of internodes throughout development.

Results

Stem morphology shifts from base to shoot tip

To evaluate the relationship between cortical microtubules (CMTs) orientation and the development of the right-handed twining phenotype, we first identified distinct morphological stages of common bean development *sensu* Onyenedum *et al.* (2025). From this study, stage 2 was selected to sample newly emergent seedlings developing its first internode (Fig. 1A); stage 3 to capture plants undergoing regular circumnutation at the shoot tip (Fig. 1A); and stage 5 to evaluate mature right-handed twining plants (Fig. 1A, B). We used epidermal markers such as stomata and trichomes to identify the outermost periclinal side of peeled epidermal tissue (Fig. 2A, B). CMT arrays were categorized into one of four major orientation groups—transverse (0–22.5° and 157.5–180°), right-skewed (22.5–67.5°), longitudinal (67.5–112.5°), and left-skewed (112.5–157.5°) (Fig. 3A–D). Internode elongation measurements are presented in Supplementary Fig. S1, and CMT orientation chi-square results are in Table 1.

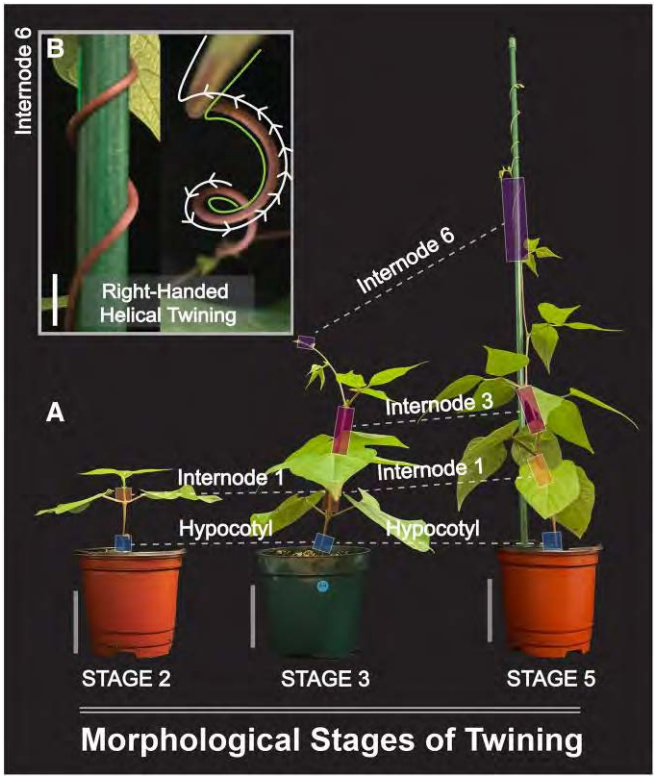

Fig. 1. Morphological stages of twining in common bean *sensu* Onyenedum *et al* (2025). (A) Sample segments–the hypocotyl, internode 1, internode 3, and internode 6–are indicated throughout three developmental stages by a shaded box. (B) Close-up of a right-handed twining at internode 6 in stage 5. Scale bars, 5 cm (A), 6.25 mm (B).

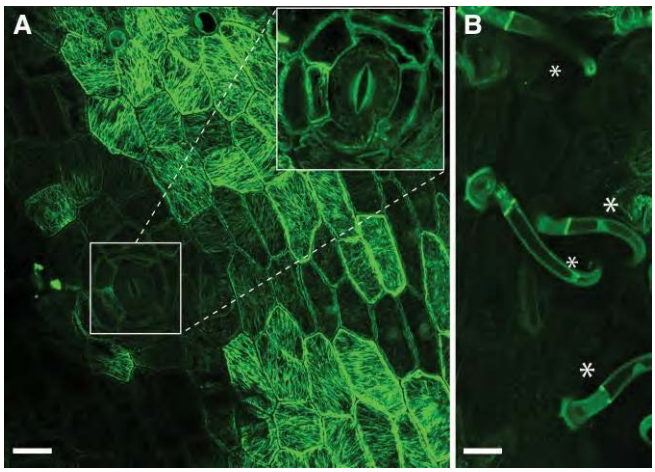

Fig. 2. Cortical microtubule arrays along the outermost periclinal face of epidermal cells in common bean. Epidermal markers, such as stomata (A) and trichomes (B) (marked with an asterisk), were used as reference points to locate the periclinal face of sampled epidermal peels. Immunostaining was performed using an anti-α-tubulin antibody excited by a 488 nm laser. Scale bars, 25 μm.

Cortical microtubules are mostly mixed and longitudinal in expanding and fully elongated internodes, respectively

Stage 2 cortical microtubule orientation of stationary basal stem segments

In stage 2, young plants are erect and short and comprise a stationary aboveground hypocotyl, epicotyl, and internode 1 (Fig. 1A). At this stage, we compared the CMT orientations in the fully elongated hypocotyl (mean±SD=2.67±0.47 cm, n=7), to the newly emergent internode 1 (mean±SD=1.34 ±0.19 cm, n=7). In the hypocotyl (Fig. 3E, 'Hypocotyl'), CMT orientations were primarily longitudinal (63.33%), with significant over-representation confirmed by chi-square analysis (Table 1). By contrast, there was no dominant angle category for CMT within the short developing internode 1 (Fig. 3E, 'Internode 1'; Table 1).

Stage 3 cortical microtubule orientation of dynamic and intermediary stem segments

In stage 3, plants underwent regular circumnutation and comprised about seven internodes (Fig. 1A). The hypocotyl, epicotyl, internode 1, and internode 2 were stationary, while internodes 4–7 underwent regular circumnutation, characterized by oscillating movement of the shoot. Internode 3 was an intermediary stem segment between the stationary base and dynamic apical internodes. By this stage, internode 1 (mean±SD length 2.25±0.45 cm, n=9) and internode 3 (mean±SD length 3.91±1.09 cm, n=9) had fully elongated, while internode 6 (mean±SD length 1.93±1.11 cm, n=9) was still elongating (Supplementary Fig. S1).

Like the previous stage, the straight hypocotyl's dominant CMT orientation remained longitudinal (51.11%) (Fig. 3F, 'Hypocotyl'; Table 1). In fully elongated internode 1, the CMT orientations shifted to a dominant longitudinal (45.6%) CMT orientation (Fig. 3F, 'Internode 1'; Table 1). The fully elongated internode 3 had a dominant longitudinal (59.33%) CMT orientation (Fig. 3F, 'Internode 3'; Table 1). Lastly, the newly emerged internode 6 had mixed CMT orientations, with no dominant angle (Fig. 3F, 'Internode 6'; Table 1).

Stage 5 cortical microtubule orientation of the matured twined stem

In stage 5, basal segments, such as the hypocotyl and internode 1, remained straight and stationary. Internode 3, the intermediary segment, transitioned from straight and dynamic to straight and stationary (Onyenedum *et al.*, 2025). Internode 6, the most apical region, transitioned from short and circumnutating to elongated and twined with the assistance of a stake (mean±SD length 10.53±3.19 cm, n=14; Supplementary Fig. S1).

Compared with the previous two stages, the straight hypocotyl's dominant CMT orientation shifted away from being longitudinally dominant to over-representation of both longitudinal (48.89%) and left-skewed (46.67%) (Fig. 3G, 'Hypocotyl'; Table 1). Internode 1 returned to a mixed grouping, with no dominant CMT orientation (Fig. 3G, 'Internode 1';

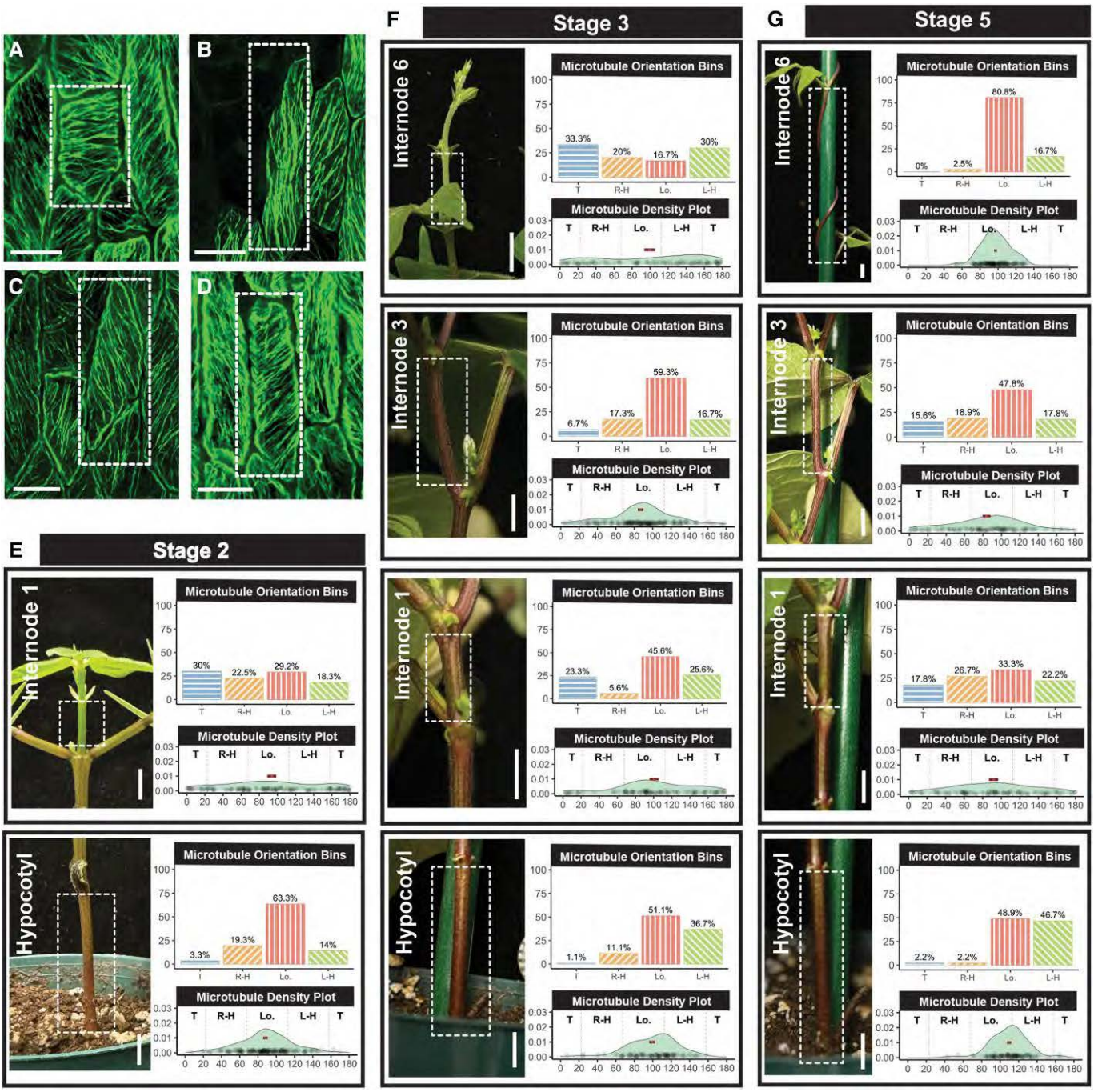

Fig. 3. Cortical microtubule (CMT) orientation bins, and their distribution in the hypocotyl, internode 1, internode 3, and internode 6 through three morphological stages of common bean. (A–D) CMT arrays binned based on the net orientation of the outermost cell wall: (A) transverse CMTs, (B) longitudinal CMTs, (C) left-skewed CMTs, and (D) right-skewed CMTs. (E–G) Representative stem segment images, and the corresponding CMT measurements grouped into four orientation bins (barplots and percentages) and the full measurement distribution (density plot) in three morphological stages: stage 2 (E), stage 3 (F), and stage 5 (G). Barplots: T, transverse (0–22.5° and 157.5–180°); R-H, right-skewed (22.5–67.5°); Lo., longitudinal (67.5–112.5°); L-H, left-skewed (112.5–157.5°). Density plot: white dot, mean CMT orientation; horizontal red bar, SE; vertical red dashed lines, boundaries between each CMT bin group. Scale bars, 25 μm (A–D), 1 cm (E–G). Measurements were obtained from 30 cells per internode at each developmental stage, using 3–5 biological replicates.

Table 1). Internode 3 CMT orientations remained significantly over-represented in the longitudinal category (47.8%) (Fig. 3G, 'Internode 3'; Table 1). Finally, within the twined internode 6, CMT orientations was significantly over-represented in the longitudinal category (80.83%) (Fig. 3G, 'Internode 6'; Table 1).

Table 1. Microtubule orientation chi-square test across three developmental stages

Stage	Tissue	No. of biological replicates	Total no. of cells measured	Chi-square residuals[a]				Dominant category/ significance
				Transverse	Right-skewed	Longitudinal	Left-skewed	
2	Hypocotyl	5	150	−6.13	−1.6	10.84	−3.11	Longitudinal (highly significant)
2	Internode 1	4	120	1.26	−0.63	1.05	−1.69	No significant deviation
3	Hypocotyl	3	90	−5.23	−3.04	5.72	2.56	Longitudinal (significant)
3	Internode 1	3	90	−0.37	−4.26	4.5	0.12	Longitudinal (significant)
3	Internode 3	5	150	−5.19	−2.17	9.71	−2.36	Longitudinal (highly significant)
3	Internode 6	3	90	1.83	−1.1	−1.83	1.1	No significant deviation
5	Hypocotyl	3	90	−4.99	−4.99	5.23	4.75	Longitudinal, left-skewed (significant)
5	Internode 1	3	90	−1.58	0.37	1.83	−0.61	No significant deviation
5	Internode 3	3	90	−2.07	−1.34	4.99	−1.58	Longitudinal (significant)
5	Internode 6	4	120	−6.32	−5.69	14.12	−2.11	Longitudinal (highly significant)

A total of 30 cells were measured for each biological replicate. [a]Residuals >±1.96 indicate significant deviation at $P<0.05$. Residuals >±2.58 indicate significant deviation at $P<0.01$.

Broadly, internodes that had not yet completed elongation (internode 1 at stage 2 and internode 6 at stage 3) displayed a mix of CMT orientations, with the largest presence of transverse CMT grouping compared with other stages (Fig. 3E, F). In contrast, segments that had just completed elongation, including the hypocotyl (stage 2), internode 1 (stage 3), internode 3 (stage 3), and internode 6 (stage 5), all displayed a dominant longitudinal CMT orientation (Fig. 3E–G; Table 1). Post-elongation stages of hypocotyl (stage 3, stage 5) and internode 1 (stage 5) revealed a subtle transition from longitudinal patterning to an increased proportion of skewed orientations (left- and/or right-skewed). Additionally, it can be noted when tracking skewed orientation groups at stage 5, internodes 1 and 3 possessed relatively equal proportions of left- and right-skewed CMT orientations, whereas the hypocotyl and internode 6 were biased towards left-skewed orientations.

Undulated stem morphology corresponds to the distribution of oblong and rounded cells

While sectioning each stem segment throughout stages 2, 3, and 5, we observed variations in cross-sectional morphology of the hypocotyl, internode 1, internode 3, and internode 6 (Fig. 4A). The hypocotyl emerged circular and remained circular, while subsequent internodes emerged slightly undulated, containing protrusions associated with cortical tissue surrounding the vascular bundles and pericyclic fibers. These subtle protrusions, referred to as 'lobes', were separated by shallow grooves termed 'furrows' that run along the main axis of the stem (Fig. 4B, C). This lobular morphology begins mildly in internode 1, whereas the hypocotyl remains circular (Fig. 4A, C). Given the realization that the stem circumference was not homogeneous, we sought to understand if there is a relationship between the configuration of the internode (straight vs. coiled), the contrast between lobes/furrows, cell shape, and CMT orientation. Towards this aim, we sampled twined plants in stage 5 and characterized cell morphologies (cell area, circularity, and geodesic diameter) and CMT angles at internode 1, internode 3, and internode 6, separating the 'lobes' from the 'furrows'. Hypocotyls were excluded given the lack of undulation.

In internode 1, epidermal cell area in the furrows and lobes was not statistically distinct ($P=0.95$; Fig. 5A). However, cells in the furrow had higher circularity than those in the lobes ($P<2.22\times10^{-16}$; Fig. 5B), and a smaller geodesic diameter, that is, a measure of length of the maximal axis ($P<2.22\times10^{-16}$; Fig. 5C). In internode 3, cell areas remained similar between the lobes and furrows ($P=0.076$; Fig. 5D), while furrows maintained a higher circularity score ($P<2.22\times10^{-16}$; Fig. 5E) and significantly smaller geodesic diameter than the lobes ($P<2.22\times10^{-16}$; Fig. 5F). In the twined internode 6, this pattern continued; cell areas remained similar ($P=0.47$; Fig. 5G), cells in the furrows continued to have higher circularity values than those in the lobes ($P=9.8\times10^{-7}$; Fig. 5H), and furrows exhibited a smaller diameter than lobes ($P=0.00042$; Fig. 5I), although this distinction was notably less pronounced than in internodes 1 and 3.

Taken together, the cell area is the same across both furrows and lobes in all three internodes examined, and thus the morphological distinction between those regions in internodes 1, 3, and 6 comes down to a distinction in circularity and geodesic diameter. Interestingly, those distinctions became less pronounced in twined internode 6, where cells were more uniformly rectangular, appearing 'stretched' (Fig. 6A).

To evaluate the association between CMT orientation and cell morphogenesis, epidermal cells were re-grouped based on their position within the furrows or lobes of internodes 1 and 3 in twined stage 5 plants using 30 cells per each of the

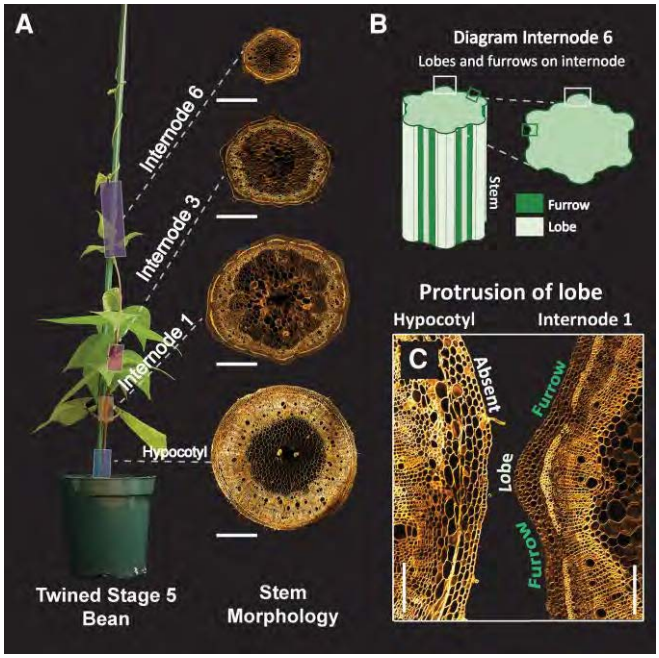

Fig. 4. Characterizing stem morphology at stage 5 of common bean. (A) Cross-sections of stem segments showing the circular outline of the hypocotyl, and subtle undulation of internodes 1, 3, and 6. (B) Illustration of the longitudinal and cross-sectional distribution of lobes and furrows at internode 6. (C) Comparison of hypocotyl and internode 1 demonstrating a lack of lobes in the former, and presence of shallow lobes in the latter. Scale bars, 500 μm (A), 125 μm (C). Cross sections stained in 0.01% (w/v) S4B.

three to five biological replicates (Table 1). Internodes 1 and 3 were selected due to the drastic differences in circularity and geodesic diameter observed between the lobes and furrows (Fig. 5). By analysing these regions separately, we found that within internode 1, the furrows and lobes comprised a mixture of CMT orientations (Fig. 6B), with no orientation bin over-represented in a chi-square residual test (Table 2). Internode 3 furrows and lobes also contained a mixture of CMT angles, with an over-representation of longitudinal CMTs in both furrows (38.8%) and lobes (73.9%) at binning (Fig. 6C, E; chi-square results in Table 2).

Discussion

This study draws inspiration from the prevailing hypothesis in the literature that the helical growth of Arabidopsis twisted mutants is shaped by the cytoskeleton. A major conclusion derived from this literature is that cortical microtubules are implicated in skewed helical growth through microtubule-associated proteins (e.g. *spiral1*, *tortifolia/spiral2*), α- and β-tubulin mutations (e.g. *TUA*, *TUB*), and microtubule-disrupting drug sensitivity (e.g. propyzamide, PSH1) (Naoi and Hashimoto, 2004; Nakajima *et al.*, 2006; Ishida *et al.*, 2007). By sampling plants expressing a twisted phenotype, a consensus has emerged that the skewed orientation of microtubules is often perpendicular to the direction of cell and overall organ growth (Smyth, 2016; Buschmann and Borchers, 2020). The first and, to our knowledge, only work examining microtubule orientation in a naturally twining species was conducted in *Ipomoea nil* with a preliminary dataset strikingly similar to twisted Arabidopsis mutants (Sousa-Baena *et al.*, 2021). These works helped to form our initial hypothesis that the right-handed growth of common bean vines likely traced back to a predominance of left-skewed microtubules in the epidermis—the main tissue layer responsible for organ formation (Kutschera and Niklas, 2007; Wada, 2012). We approached this study by sampling not only twined plants at maturity, but also re-sampling the four stem segments (hypocotyl, internodes 1, 3, and 6) throughout plant maturation from a seedling (stage 2) to early circumnutation (stage 3) to a coiled adult (stage 5). Therefore, our results not only inform us about the association between microtubule orientation and coiled internodes but also about how microtubule patterning changes as an internode elongates, undergoes regular circumnutation, and eventually coils.

Are skewed microtubules associated with twining?

To our surprise, we did not find a dominance of skewed microtubules at any stage, thus refuting our initial hypothesis. Instead, we found that fully elongated internodes, both straight and coiled, exhibited predominantly longitudinal microtubules. Meanwhile, still elongating internodes displayed a mixture of arrangements, with the highest frequency of transversal orientation occurrence (Fig. 3E, 'Internode 1'; Fig. 3G, 'Internode 6'). This observation provides support for earlier findings that cortical microtubules and cellulose microfibrils often align transversely to the growth axis (Green, 1962), a phenomenon also noted in 10-day-old *Ipomoea nil* hypocotyls (Sousa-Baena *et al.*, 2021). However, we found a left-skewed over right-skewed bias in the hypocotyl and internode 6, albeit this left-skewed bias always took second place to the dominant longitudinal pattern (Fig. 3G, 'Hypocotyl' and 'Internode 6'). Interestingly, both stem segments demonstrate the capacity for twisting—just as observed in the hypocotyl during shoot emergence from the soil (Supplementary Fig. S2), and across internode 6, which both twines and twists (Fig. 1B). This preference aligns with existing knowledge of directional cell expansion (Baskin, 2005), suggesting a link between left-skewed microtubule orientation and right-handed cell files. In contrast, straight stem segments, internodes 1 and 3, were relatively at equilibrium between right- and left-skewed microtubules, with the only exception being internode 1 (stage 3) when it is undergoing circumnutation (Fig. 3E–G). If skewed microtubule orientation indeed reflects organ chirality in twining vines, our findings suggest it emerges later in development, after elongation. Nonetheless, given the dominance of the

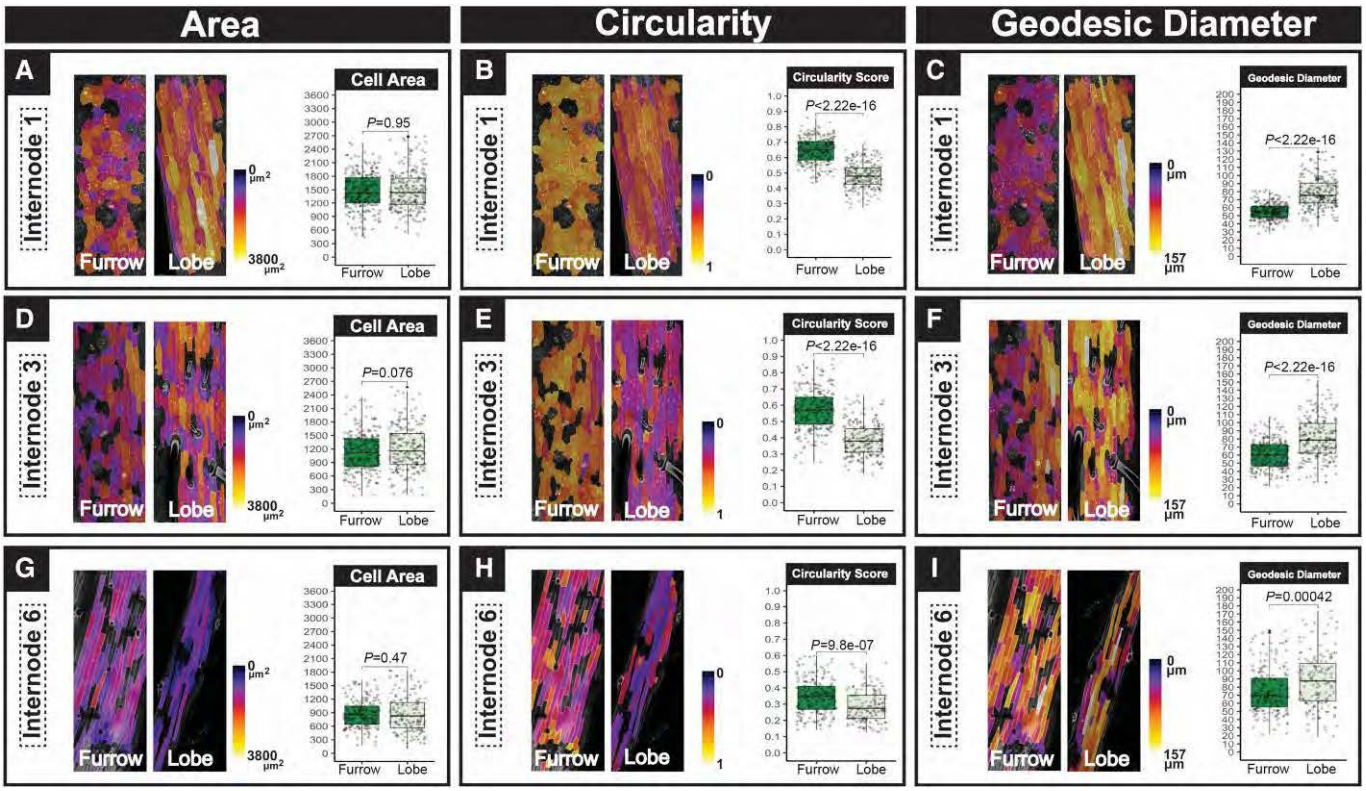

Fig. 5. Cell morphologies across furrows and lobes in stage 5 twined common bean. Epidermal peels of internode 1 (A–C), internode 3 (D–F), and internode 6 (G–I) were evaluated based on their position in the lobe or furrow. Individually segmented cells were measured based on their cell area (0–3800), circularity score, that is, roundness of cells (0–1), and geodesic diameter, that is, the length of the longest axis of the cell accounting for cell convexity (0–157 µm). Statistical significance was evaluated using the Wilcoxon rank-sum tests coupled with the Bonferroni *P*-adjustment method ($P<0.05$, Mann-Whitney *U*-test) in boxplots. Measurements were obtained from at least 30 cells per internode at each developmental stage for each of the three biological replicates.

longitudinal microtubule patterning found, we will focus below on alternative hypotheses explaining this pattern.

Longitudinal microtubules may reflect tension across stretched twined internodes

So why are cortical microtubules aligned longitudinally in twined internodes? One cause for the broad dominance of longitudinal patterning would be the potential for dynamic CMT rearrangement in response to external stimuli. While hyper-responsiveness to tensile stress is innately curbed via microtubule-associated kinases (i.e. NEK6; Takatani *et al.*, 2020), sufficient mechanical damage (Sampathkumar *et al.*, 2014), nutrient acquisition (Sheng *et al.*, 2024), and/or tension and compression patterns applied across plant tissue (Hejnowicz *et al.*, 2000; Hamant *et al.*, 2008) can cause shifts in microtubule arrangement. Even growth signals such as rootword hypocotyl expansion have been shown to induce longitudinal arrangements in *nek6* Arabidopsis mutants via exaggerated responsiveness (Takatani *et al.*, 2020). It should be noted that even with NEK6 presence, innate growth cues are common internal stresses that influence microtubule arrangements. In the case of twiners, we suspect that significant tensile and compressive forces caused by climbing may be causing reorientation to align parallel to the direction of maximal force, as observed in other plant tissue types (Sahaf and Sharon, 2016; Robinson and Kuhlemeier, 2018; Zhao *et al.*, 2020).

As a twining plant ascends a support structure, tensile stresses naturally occur. A circumnutating stem must supply ample grip to secure contact with a support and counteract gravitational forces, consequently stretching the stem along the length of the support (Fig. 6A) (Silk and Hubbard, 1991; Silk and Holbrook, 2005; Isnard *et al.*, 2009). Furthermore, according to the main stages of tension identified by Isnard *et al.* (2009), a stipule-assisted climber, *Discorea bulbifera*, can experience up to 150 mN in squeezing forces when coiled around a pole. Considering the similarities of *D. bulbifera* to twining common bean, we predict that twined internode 6 likely undergoes comparable squeezing forces. In Arabidopsis, tensile and compressive applied forces as low as 1.5–2 mN were sufficient to induce microtubule realignment from transverse to longitudinal in the hypocotyl (Robinson and Kuhlemeier, 2018). Therefore, if common bean experienced comparable tensile forces induced by climbing a host, these stresses could drive substantial microtubule rearrangement.

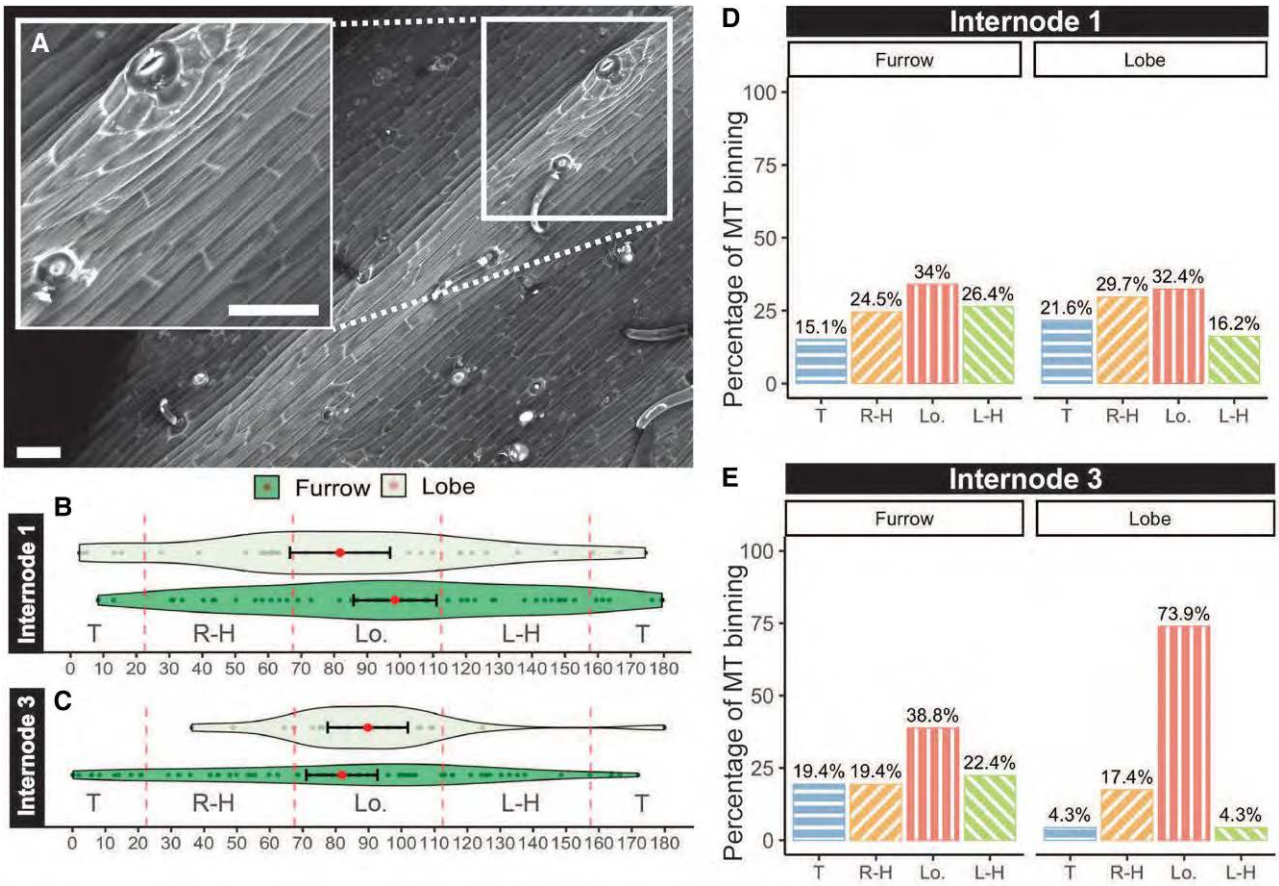

Fig. 6. Cell morphologies and cortical microtubule angles in common bean. (A) Rectangular cell morphologies were found along a twined internode 6 in stage 5. These cells possess vertical striations along their cell wall and are presumably caused by the stretching of the organ whilst twining. Confocal scan of sample stained with 10 μg ml^{-1} propidium iodide. Scale bar, 50 μm. (B–E) Cortical microtubule (CMT) orientation data separated by furrows and lobes in internodes 1 and 3 displayed as violin plots or barplots in twined plats in stage 5. (B) Violin plot of internode 1 showing CMT orientation distribution, mean (red dot), and confidence interval (horizontal red line). Vertical red dashed lines indicate boundaries between each binning category: T, transverse (0–22.5° and 157.5–180°); R-H, right-skewed (22.5–67.5°); Lo., longitudinal (67.5–112.5°); L-H, left-skewed (112.5–157.5°). (C) Violin plot of internode 3. (D) Bar plot of internode 1 showing the percentage of each CMT orientation bin. (E) Bar plot of internode 3. Measurements were obtained from at least 23 cells per internode using three biological replicates.

Longitudinal microtubules may reflect secondary growth of the stationary internodes

Longitudinal patterning in basal, straight stem segments like the hypocotyl, internode 1, and internode 3, cannot be readily explained by twining-related tension. Instead, we propose that the expansion of inner tissue by secondary growth drives this microtubule arrangement. As the common bean stem thickens post-elongation, vascular expansion from secondary growth exerts pressure on outer tissues, particularly the epidermis. Similarly, the epidermal growth theory ('tensile skin theory') highlights the bidirectional stresses exchanged between inner and outer tissues (Kutschera, 1989; Hejnowicz and Sievers, 1995). Supporting this theory, studies on sunflower hypocotyls demonstrated an increased inner tissue growth of 15% due to the release of external epidermal constraints (Hejnowicz *et al.*, 2000; Kutschera and Niklas, 2007). These findings emphasize the role of the epidermis in shaping organs and managing axial growth forces exerted by internal tissues. However, in radial expansion, the thickening of vascular tissue is capable of generating circumferential strain on the stem and serving as a growth directional cue for the organ, similar to commonly studied axial growth (Baskin and Jensen, 2013). Thus, post-elongation longitudinal microtubule arrangement likely facilitates epidermal vertical expansion, enabling the tissue to counteract internal radial pressure from secondary growth while preserving the structural integrity of the organ.

Exploring the possible stressors causing internal tissue expansion led us to question whether cortical microtubule orientation on the innermost periclinal face (facing the cortex) differed from those on the outmost face, facing the wavy cuticle (Supplementary Fig. S3). In Arabidopsis, inner and outer epidermal faces of CMTs often differ, with inner faces reflecting growth directionality compared with

Table 2. Microtubule orientation Chi-square test comparing lobes and furrows in developmental stage 5

Tissue	Lobe vs. Furrow	No. of biological replicates	Total no. of cells measured	Chi-square residuals[a]				Dominant category/ significance
				Transverse	Right-skewed	Left-skewed	Longitudinal	
Internode 1	Lobe	3	37 cells	−0.47	0.66	−1.23	−1.23	No significant deviation
Internode 1	Furrow	3	53 cells	−1.67	−0.079	0.23	1.51	No significant deviation
Internode 3	Lobe	3	23 cells	−2.28	−0.84	−2.28	5.41	Longitudinal (significant)
Internode 3	Furrow	3	67 cells	−1.06	−1.06	−0.50	2.6	Longitudinal (significant)

Measurements from plants in Table 1 were regrouped based on their positioning in either the lobe of furrow of an internode. [a]Residuals >±1.96 indicate significant deviation at $P<0.05$. Residuals >±2.58 indicate significant deviation at $P<0.01$.

transient orientation shifts on the outer surface (Crowell *et al.*, 2011). By contrast, in common bean hypocotyls, we observed consistent orientations across both faces, with longitudinal CMTs dominating at all three developmental stages (Supplementary Fig. S3). Notably, the inner face mirrored the left-handed skewing of the outer epidermis, with the exception of stage 5, where the inner faces displayed slight right-handed skewing. These preliminary findings suggest that common bean mostly exhibits comparable CMT distributions across inner and outer epidermal faces amidst internal growth cues, differing from Arabidopsis, where inner–outer facing orientations vary with developmental progress.

Distribution of oblong and rounded cell morphologies across the stem periphery

While examining common bean morphology, we observed a transition from a circular basal stem to a slightly undulating, noncircular stem in distal internodes (Fig. 4). Protrusions along the stem periphery correlated with a thicker cortex and positioning of pericyclic gelatinous fibers, which generate localized areas of tensile stress and reinforce stem posture (Mellerowicz *et al.*, 2008; Mellerowicz and Gorshkova, 2012; Onyenedum *et al.*, 2025). The transition between stem morphologies may serve distinct purposes in posture maintenance: the circular basal hypocotyl has a prominent role during self-supporting growth, while the more distal internodes develop protruding 'lobes' and recessed 'furrows' (Fig. 4A) that may assist with early flexibility required in twining. Their shape is similar to other climbing plants with non-circular stems, such as *Bauhinia* sp. and *Paullina* spp. (Bhambie, 1972; Rowe and Speck, 2005; Isnard and Silk, 2009; Chery *et al.*, 2020).

These implications emphasize the functionality of 'lobes' and 'furrows' concerning twining, and prompted us to assess their composition at the cellular level. Along the stem perimeter, we also found distinct cell morphologies between the lobes and furrows. Lobes contained rectangular-shaped cells, while furrows had round-shaped cells, the latter becoming relatively more rectangular (Fig. 5) and stretched in apically twined internodes (Fig. 6A). These differences suggest variations of isotropic and anisotropic cell growth between the two regions—however, the microtubule organization patterns found suggest an added layer of complexity to cell formation. During post-elongation, stage 5, internode 1 lacked a clear distinction in microtubule orientation between the lobe and furrow (Fig. 6D); meanwhile, the lobe of internode 3 demonstrated a notably higher affinity for longitudinal arrangement at 73.9% compared with the furrow with 38.8% (Fig. 6E). These observations suggest that common bean stems compartmentalize cell growth to create a structure that is initially self-supporting and then well-adapted for climbing. However, we were unable to pinpoint microtubule arrangement as the definitive origin of variability in lobes and furrows; this complexity lies in the dynamic nature of microtubule arrangement that shifts amidst both internal growth and external mechanical stress and damage.

Free-standing twisting organs versus helical twining along a support

Although Arabidopsis mutants have laid the groundwork for investigating microtubule-driven twisting, key differences exist between 'twisting' versus 'twining'. A useful analogy is a shoestring fixed at one end: in twisting, the free end is twirled, creating a drill-bit shape. In contrast, twining occurs when the shoestring stretches its axis, wrapping around a support, forming a spring-like coil. Arabidopsis twisted mutants exhibit skewed directional growth at the cellular and organ levels, evidenced by twisted epidermal cell files (Thitamadee *et al.*, 2002; Ishida *et al.*, 2007) and individual cells (Verger *et al.*, 2019). In contrast, twining plants like common bean must elongate and slightly twist as a mechanical necessity when twining (Darwin, 1875; Isnard *et al.*, 2009). This twisting is less pronounced than in Arabidopsis mutants, where millimeter-sized organs exhibit drastic cell file skewing (Furutani *et al.*, 2000; Thitamadee *et al.*, 2002; Nakajima *et al.*, 2004). Instead of extreme cell file twisting, twined epidermal cells appear more longitudinally stretched (Fig. 6A), likely due to organ-level stress imposed during climbing. Moreover, twining plants do not rely solely on twisting to maintain their helical structure—they require constant support contact for early posture adherence via thigmotropism (Huberman and Jaffe, 1986; Onyenedum *et al.*, 2025). For instance, once circumnutating internodes

establish unilateral contact with a stake, emerging internodes use the support as a guide, simultaneously twining and elongating into a coiled position. Taken together, the clear dominance of skewed microtubules in Arabidopsis and the lack thereof in common bean may reflect two different modes of helical growth: cells grow in a twisted manner to form twisted organs in Arabidopsis, versus the internode must both elongate and grow in a helical fashion while in contact with a support in common bean.

Our findings suggest that CMTs are more reflective of the complex suite of stresses associated with climbing, rather than serving as a sole predictor of organ chirality. This highlights the need to investigate how cytoskeletal behavior integrates multiple cues—including mechanical friction, helical growth, and secondary growth—into shaping the twining habit. For instance, CMT responsiveness to stress may involve hyper-responsiveness regulators similar to NEK6 in Arabidopsis (Takatani *et al.*, 2020), or the development of tropism responses via auxin localization as observed in Arabidopsis root structures (Adamowski and Friml, 2015). Beyond the cytoskeleton, the cell wall may also play a significant role. In Arabidopsis, a novel left-handed twining phenotype arose not from altered CMTs, but from decreased levels of the pectic polysaccharide rhamnogalacturonan-I, demonstrating that multiple pathways can underlie twining growth (Saffer *et al.*, 2017).

Supplementary data

The following supplementary data are available at *JXB* online.

Fig. S1. Internode elongation throughout developmental stages.

Fig. S2. The twisting of the hypocotyl in common bean seedlings resembles the self-twisting nature of Arabidopsis twisted mutants.

Fig. S3. Cortical microtubule orientations in the inner and outer epidermal face in the hypocotyl of common bean.

Acknowledgements

A special thank you to all Onyenedum lab members—Lena Hunt, Israel L. Cunha-Neto, Zachary Kozma, Hannah Ratcliff, Yifan Wang, Annabelle Wang, and Leo Semana—for their unconditional support and advice with experiments, revisions, and, of course, plant care.

Author contributions

JGO, MSSB, and AAA: conceptualization; MSSB and AAA: methodology; AAA: investigation; JGO and AAA: formal analysis; JGO: resources; AAA: data curation; JGO and AAA: scripts; JGO and AAA: writing—original draft; AAA, MSSB, and JGO: writing—review & editing; JGO and AAA: visualization; JGO supervision; JGO: funding acquisition.

Conflict of interest

The authors declare they have no competing interests.

Funding

This work was largely supported by NSF CAREER award #2401675 under JGO. Preliminary Immunolocalization experiments conducted at Cornell University received support from laboratory startup funds under JGO.

Data availability

Cortical microtubule datasets and internode elongation measurements are published on Zenodo (Acevedo, 2025) while associated scripts are available at https://github.com/angelique-acevedo/Microtubule-Twining-Analysis.

References

Acevedo A. 2025. Data from: Helical growth of twining common bean is associated with longitudinal, not skewed, microtubule patterning. Zenodo. https://doi.org/10.5281/zenodo.17082352

Adamowski M, Friml J. 2015. PIN-dependent auxin transport: action, regulation, and evolution. The Plant Cell **27**, 20–32.

Anderson CT, Carroll A, Akhmetova L, Somerville C. 2010. Real-time imaging of cellulose reorientation during cell wall expansion in Arabidopsis roots. Plant Physiology **152**, 787–796.

Baskin TI. 2005. Anisotropic expansion of the plant cell wall. Annual Review of Cell and Developmental Biology **21**, 203–222.

Baskin TI, Jensen OE. 2013. On the role of stress anisotropy in the growth of stems. Journal of Experimental Botany **64**, 4697–4707.

Bhambie S. 1972. Correlation between form, structure and habit in some lianas. Proceedings of the Indian Academy of Sciences **75**, 246–256.

Boudaoud A, Burian A, Borowska-Wykręt D, Uyttewaal M, Wrzalik R, Kwiatkowska D, Hamant O. 2014. FibrilTool, an ImageJ plug-in to quantify fibrillar structures in raw microscopy images. Nature Protocols **9**, 457–463.

Buschmann H, Fabri CO, Hauptmann M, Hutzler P, Laux T, Lloyd CW, Schäffner AR. 2004. Helical growth of the *Arabidopsis* mutant *Tortifolia1* reveals a plant-specific microtubule-associated protein. Current Biology **14**, 1515–1521.

Buschmann H, Hauptmann M, Niessing D, Lloyd CW, Schäffner AR. 2009. Helical growth of the *Arabidopsis* mutant *Tortifolia2* does not depend on cell division patterns but involves handed twisting of isolated cells. The Plant Cell **21**, 2090–2106.

Buschmann H, Borchers A. 2020. Handedness in plant cell expansion: a mutant perspective on helical growth. New Phytologist **225**, 53–69.

Celler K, Fujita M, Kawamura E, *et al*. 2016. Microtubules in plant cells: strategies and methods for immunofluorescence, transmission electron microscopy, and live cell imaging. In: **Gavin RH**, ed. Cytoskeleton methods and protocols. Methods in Molecular Biology, Vol. **1365**. New York: Humana Press, 155–184.

Chery JG, da Cunha Neto IL, Pace MR, Acevedo-Rodríguez P, Specht CD, Rothfels CJ. 2020. Wood anatomy of the neotropical Liana lineage *Paullinia* L. (Sapindaceae). IAWA Journal **41**, 278–300.

Crowell EF, Timpano H, Desprez T, Franssen-Verheijen T, Emons A-M, Höfte H, Vernhettes S. 2011. Differential regulation of cellulose orientation at the inner and outer face of epidermal cells in the *Arabidopsis* hypocotyl. The Plant Cell **23**, 2592–2605.

Darwin C. 1875. The movements and habits of climbing plants. London: John Murray.

Duncombe SG, Chethan SG, Anderson CT. 2022. Super-resolution imaging illuminates new dynamic behaviors of cellulose synthase. The Plant Cell **34**, 273–286.

Edwards W, Moles AT, Franks P. 2007. The global trend in plant twining direction. Global Ecology and Biogeography **16**, 795–800.

FC M, Davis T, ggplot2 authors. 2022. *ggpattern: 'ggplot2' Pattern Geoms*. https://github.com/coolbutuseless/ggpattern

Furutani I, Watanabe Y, Prieto R, Masukawa M, Suzuki K, Naoi K, Thitamadee S, Shikanai T, Hashimoto T. 2000. The *SPIRAL* genes are required for directional control of cell elongation in *Arabidopsis thaliana*. Development **127**, 4443–4453.

Green PB. 1962. Mechanism for plant cellular morphogenesis. Science **138**, 1404–1405.

Hamant O, Heisler MG, Jönsson H, *et al.* 2008. Developmental patterning by mechanical signals in *Arabidopsis*. Science **322**, 1650–1655.

Heath IB. 1974. A unified hypothesis for the role of membrane bound enzyme complexes and microtubules in plant cell wall synthesis. Journal of Theoretical Biology **48**, 445–449.

Hejnowicz Z, Sievers A. 1995. Tissue stresses in organs of herbaceous plants: I. Poisson ratios of tissues and their role in determination of the stresses. Journal of Experimental Botany **46**, 1035–1043.

Hejnowicz Z, Rusin A, Rusin T. 2000. Tensile tissue stress affects the orientation of cortical microtubules in the epidermis of sunflower hypocotyl. Journal of Plant Growth Regulation **19**, 31–44.

Huberman M, Jaffe MJ. 1986. Thigmotropism in organs of the bean plant (*Phaseolus vulgaris* L.). Annals of Botany **57**, 133–137.

Ishida T, Kaneko Y, Iwano M, Hashimoto T. 2007. Helical microtubule arrays in a collection of twisting tubulin mutants of *Arabidopsis thaliana*. Proceedings of the National Academy of Sciences, USA **104**, 8544–8549.

Isnard S, Cobb AR, Holbrook NM, Zwieniecki M, Dumais J. 2009. Tensioning the Helix: a mechanism for force generation in twining plants. Proceedings of the Royal Society of London: Series B, Biological Sciences **276**, 2643–2650.

Isnard S, Silk WK. 2009. Moving with climbing plants from Charles Darwin's time into the 21st century. American Journal of Botany **96**, 1205–1221.

Kassambara A. 2023. *ggpubr: 'ggplot2' Based Publication Ready Plots*. R package version 0.6.0, https://rpkgs.datanovia.com/ggpubr/

Kutschera U. 1989. Tissue stresses in growing plant organs. Physiologia Plantarum **77**, 157–163.

Kutschera U, Niklas KJ. 2007. The epidermal-growth-control theory of stem elongation: an old and a new perspective. Journal of Plant Physiology **164**, 1395–1409.

Legland D, Arganda-Carreras I, Andrey P. 2016. MorphoLibJ: integrated library and plugins for mathematical morphology with ImageJ. Bioinformatics **32**, 3532–3534.

Liang BM, Dennings AM, Sharp RE, Baskin TI. 1996. Consistent handedness of microtubule helical arrays in maize and *Arabidopsis* primary roots. Protoplasma **190**, 8–15.

Medina MC, Sousa-Baena MS, Van Sluys M-A, Demarco D. 2022. Laticifer growth pattern is guided by cytoskeleton organization. Frontiers in Plant Science **13**, 971235.

Mellerowicz EJ, Immerzeel P, Hayashi T. 2008. Xyloglucan: the molecular muscle of trees. Annals of Botany **102**, 659–665.

Mellerowicz EJ, Gorshkova TA. 2012. Tensional stress generation in gelatinous fibres: a review and possible mechanism based on cell-wall structure and composition. Journal of Experimental Botany **63**, 551–565.

Nakajima K, Furutani I, Tachimoto H, Matsubara H, Hashimoto T. 2004. *SPIRAL1* encodes a plant-specific microtubule-localized protein required for directional control of rapidly expanding Arabidopsis cells. The Plant Cell **16**, 1178–1190.

Nakajima K, Kawamura T, Hashimoto T. 2006. Role of the *SPIRAL1* gene family in anisotropic growth of *Arabidopsis thaliana*. Plant & Cell Physiology **47**, 513–522.

Naoi K, Hashimoto T. 2004. A semidominant mutation in an *Arabidopsis* mitogen-activated protein kinase phosphatase-like gene compromises cortical microtubule organization. The Plant Cell **16**, 1841–1853.

Neuwirth E. 2022. *RColorBrewer: ColorBrewer Palettes*. R package version 1.1-3, https://cran.r-project.org/web/packages/RColorBrewer/index.html

Onyenedum JG, Sousa-Baena MS, Hunt LM, Acevedo AA, Glos RAE, Anderson CT. 2025. Gelatinous fibers develop asymmetrically to support bends and coils in common bean vines (*Phaseolus vulgaris*). American Journal of Botany **112**, e70014.

Paredez AR, Somerville CR, Ehrhardt DW. 2006. Visualization of cellulose synthase demonstrates functional association with microtubules. Science **312**, 1491–1495.

Renou J, Li D, Lu J, *et al.* 2024. A cellulose synthesis inhibitor affects cellulose synthase complex secretion and cortical microtubule dynamics. Plant Physiology **196**, 124–136.

Robinson S, Kuhlemeier C. 2018. Global compression reorients cortical microtubules in *Arabidopsis* hypocotyl epidermis and promotes growth. Current Biology **28**, 1794–1802.e2.

Rowe N, Speck T. 2005. Plant growth forms: an ecological and evolutionary perspective. New Phytologist **166**, 61–72.

Sahaf M, Sharon E. 2016. The rheology of a growing leaf: stress-induced changes in the mechanical properties of leaves. Journal of Experimental Botany **67**, 5509–5515.

Saffer AM, Carpita NC, Irish VF. 2017. Rhamnose-containing cell wall polymers suppress helical plant growth independently of microtubule orientation. Current Biology **27**, 2248–2259.e4.

Sampathkumar A, Krupinski P, Wightman R, Milani P, Berquand A, Boudaoud A, Hamant O, Jönsson H, Meyerowitz EM. 2014. Subcellular and supracellular mechanical stress prescribes cytoskeleton behavior in *Arabidopsis* cotyledon pavement cells. eLife **3**, e01967.

Sedbrook JC, Ehrhardt DW, Fisher SE, Scheible W-R, Somerville CR. 2004. The Arabidopsis *SKU6/SPIRAL1* gene encodes a plus End–localized microtubule-interacting protein involved in directional cell expansion. The Plant Cell **16**, 1506–1520.

Sheng H, Bouwmeester HJ, Munnik T. 2024. Phosphate promotes Arabidopsis root skewing and circumnutation through reorganisation of the microtubule cytoskeleton. New Phytologist **244**, 2311–2325.

Shoji T, Narita NN, Hayashi K, Asada J, Hamada T, Sonobe S, Nakajima K, Hashimoto T. 2004. Plant-specific microtubule-associated protein SPIRAL2 is required for anisotropic growth in Arabidopsis. Plant Physiology **136**, 3933–3944.

Silk WK, Hubbard M. 1991. Axial forces and normal distributed loads in twining stems of morning glory. Journal of Biomechanics **24**, 599–606.

Silk WK, Holbrook NM. 2005. The importance of frictional interactions in maintaining the stability of the twining habit. American Journal of Botany **92**, 1820–1826.

Smyth DR. 2016. Helical growth in plant organs: mechanisms and significance. Development **143**, 3272–3282.

Sousa-Baena MS, Hernandes-Lopes J, Van Sluys M-A. 2021. Reaching the top through a tortuous path: helical growth in climbing plants. Current Opinion in Plant Biology **59**, 101982.

Takatani S, Verger S, Okamoto T, Takahashi T, Hamant O, Motose H. 2020. Microtubule response to tensile stress is curbed by NEK6 to buffer growth variation in the *Arabidopsis* hypocotyl. Current Biology **30**, 1491–1503.e2.

Thitamadee S, Tuchihara K, Hashimoto T. 2002. Microtubule basis for left-handed helical growth in *Arabidopsis*. Nature **417**, 193–196.

Verger S, Liu M, Hamant O. 2019. Mechanical conflicts in twisting growth revealed by cell-cell adhesion defects. Frontiers in Plant Science **10**, 173.

Wada H. 2012. Hierarchical helical order in the twisted growth of plant organs. Physical Review Letters **109**, 128104.

Wasteneys GO, Willingale-Theune J, Menzel D. 1997. Freeze shattering: a simple and effective method for permeabilizing higher plant cell walls. Journal of Microscopy **188**, 51–61.

Wickham H. 2016. Ggplot2: elegant graphics for data analysis. New York: Springer-Verlag. ISBN 978-3-319-24277-4, https://ggplot2.tidyverse.org

Zhao F, Du F, Oliveri H, *et al.* 2020. Microtubule-mediated wall anisotropy contributes to leaf blade flattening. Current Biology **30**, 3972–3985.e6.

Zhou W, Li D, Pšenička J, Boyce CK, Wang J. 2019. A left-handed fern twiner in a Permian swamp forest. Current Biology **29**, R1172–R1173.